OBSERVATIONAL CONSTRAINTS ON COSMOLOGICAL MODELS WITH CHAPLYGIN GAS AND QUADRATIC EQUATION OF STATE

G. S. Sharov[1]

[1] *Tver state university*
*170002, Sadovyj per. 35, Tver, Russia**

Observational manifestations of accelerated expansion of the universe, in particular, recent data for Type Ia supernovae, baryon acoustic oscillations, for the Hubble parameter $H(z)$ and cosmic microwave background constraints are described with different cosmological models. We compare the ΛCDM, the models with generalized and modified Chaplygin gas and the model with quadratic equation of state. For these models we estimate optimal model parameters and their permissible errors with different approaches to calculation of sound horizon scale $r_s(z_d)$. Among the considered models the best value of χ^2 is achieved for the model with quadratic equation of state, but it has 2 additional parameters in comparison with the ΛCDM and therefore is not favored by the Akaike information criterion.

I. INTRODUCTION

Observations [1, 2] of Type Ia supernovae demonstrated accelerated expansion of our universe. Further investigations of supernovae [3, 4], baryon acoustic oscillations [4–7], cosmic microwave background measurements [7–10], estimations [11–25] of the Hubble parameter $H(z)$ for different redshifts z confirmed accelerated growth of the cosmological scale factor $a(t)$ at late stage of its evolution.

For Type Ia supernovae we can measure their redshifts z and luminosity distances D_L, so these objects may be used as standard candles [1–4].

Baryon acoustic oscillations (BAO) are observed as a peak in the correlation function of the galaxy distribution at the comoving sound horizon scale $r_s(z_d)$ [5, 6], corresponding to the end of the drag era, when baryons became decoupled and acoustic waves propagation was ended. This effect has various observational manifestations [8–10, 16–33], in particular, one can estimate the Hubble parameter $H(z)$ for definite redshifts [16–25] (details are in Sect. II).

The mentioned recent observations of Type Ia supernovae, BAO and $H(z)$ essentially restrict possible cosmological theories and models. To satisfy these observations all models are to describe accelerated expansion of the universe with definite parameters [8–10, 34–36].

The standard Einstein gravity with $\Lambda = 0$ predicts deceleration of the expanding universe: $a''(t) < 0$. So to explain observed accelerated expansion, we are to modify this theory. The most simple (and most popular) modification is the ΛCDM, including dark energy corresponding to $\Lambda \neq 0$ and cold dark matter in addition to deficient visible matter. This model with appropriate parameters [4, 8–10] successfully describes practically all observational data, in Sect. III we apply this model to describe the updated recent observations of Type Ia supernovae, BAO effects and $H(z)$ estimates. In this paper we use the notation ΛCDM for the model with an arbitrary spatial curvature Ω_k.

One should note that there are some problems in the ΛCDM model, in particular, ambiguous nature of dark matter and dark energy, the problem of fine tuning for the observed value of Λ and the coincidence problem for surprising proximity Ω_Λ and Ω_m nowadays [35, 36].

*Electronic address: german.sharov@mail.ru

Therefore cosmologists suggested a lot of alternative models with different equations of state, scalar fields, with $f(R)$ Lagrangian, additional space dimensions and many others [35–39]. In this paper we consider in detail two models with nontrivial equations of state describing both dark matter and dark energy: the model with modified Chaplygin gas (MCG) [40–47] in Sect. IV and the model with quadratic equation of state [48–53] in Sect. V.

II. OBSERVATIONAL DATA

In this paper we use the Union2.1 compilation [3] of Type Ia supernovae (SNe Ia) observational data. This table includes redshifts $z = z_i$ and distance moduli $\mu_i = \mu_i^{obs}$ with errors σ_i for $N_{SN} = 580$ supernovae. The distance modulus $\mu_i = \mu(D_L) = 5\log_{10}(D_L/10\text{pc})$ is logarithm of the luminosity distance [1, 34, 35]:

$$D_L(z) = \frac{c\,(1+z)}{H_0} S_k\Big(H_0 \int\limits_0^z \frac{d\tilde{z}}{H(\tilde{z})}\Big). \tag{1}$$

Here

$$S_k(x) = \begin{cases} \sinh(x\sqrt{\Omega_k})/\sqrt{\Omega_k}, & \Omega_k > 0, \\ x, & \Omega_k = 0, \\ \sin(x\sqrt{|\Omega_k|})/\sqrt{|\Omega_k|}, & \Omega_k < 0; \end{cases}$$

redshift z and the Hubble parameter $H(z)$ are connected with the scale factor $a(t)$:

$$a(t) = \frac{a_0}{1+z}, \qquad H(z) = \frac{\dot{a}(t)}{a(t)}; \tag{2}$$

k is the sign of curvature, $\Omega_k = -k/(a_0^2 H_0^2)$ is its present time fraction, $a_0 \equiv a(t_0)$ and $H_0 \equiv H(t_0)$ are the current values of a and H.

For any cosmological model we fix its model parameters $p_1, p_2, \ldots$, calculate dependence $a(t)$, the integral (1) and this model predicts theoretical values D_L^{th} for luminosity distance (1) (for given z), or μ^{th} for modulus. To compare these theoretical values with the observational data z_i and μ_i^{obs} from the table [3] we use the function

$$\chi^2_{SN}(p_1, p_2, \ldots) = \min_{H_0} \sum_{i,j=1}^{N_{SN}} \Delta\mu_i (C_{SN}^{-1})_{ij} \Delta\mu_j, \qquad \Delta\mu_i = \mu^{th}(z_i, H_0, p_1, \ldots) - \mu_i^{obs}. \tag{3}$$

Here C_{SN} is the SN-by-SN covariance matrix [3], representing systematic errors.

In the sum (1) marginalization over the Hubble constant H_0 is assumed, because we have to take into account model dependence of the moduli μ_i^{obs}. Unlike observed apparent magnitudes m_i^{obs} the values μ_i^{obs} in Ref. [3] are estimated as

$$\mu^{obs} = m^{obs}(z) - M + \alpha x_1 - \beta c + \delta P. \tag{4}$$

This formula includes the SN Ia absolute magnitude M and corrections connected with deviations from mean values of lightcurve shape (x_1), SN Ia color (c) and mass of a host galaxy (the factor P). The parameters M, α, β and δ are considered in Ref. [3] as nuisance parameters, they are fitted simultaneously with the cosmological parameters in the flat ΛCDM model.

Thus we have a model dependent additive term in Eq. (4) for the Union2.1 values μ^{obs} [3] with concealed dependence on the Hubble constant H_0 and other model parameters. In particular, one

can find only that the best fit value for the absolute magnitude $M = -19.321 \pm 0.03$ is obtained in Ref. [3] for $h = 0.7$, where $h = H_0/100\ \mathrm{km\,s^{-1}Mpc^{-1}}$.

To suppress this dependence many authors [54–57] suppose that values μ_i^{obs} from any SN Ia survey have a systematic error depending on H_0 and marginalize the sum (1) over the Hubble constant H_0. They use the fact, that for the most popular models theoretical value of the luminosity distance (1) depends on H_0 as $D_L^{th} \sim H_0^{-1}$, so the distance modulus μ^{th} has the additive term $-5\log_{10} H_0$. In Ref. [54] this term is separated as μ_0 in the form

$$\mu(D_L) = 5\log_{10}\frac{H_0 D_L}{c} + \mu_0, \qquad \mu_0 = 42.384 - 5\log_{10} h;$$

if we denote $d_i = \Delta\mu_i - \mu_0$, $\mathbf{d} = (d_1, \ldots, d_{SN})$, the minimum of the sum (3) over H_0 (or over μ_0) will take the form

$$\chi^2_{SN}(p_1, \ldots) = \mathbf{d}C_{SN}^{-1}\mathbf{d}^T - \frac{B^2}{C}, \qquad B = \sum_{i,j=1}^{N_{SN}} d_i (C_{SN}^{-1})_{ij}, \quad C = \sum_{i,j=1}^{N_{SN}} (C_{SN}^{-1})_{ij}. \tag{5}$$

In this paper for all models we use the marginalized function (5) χ^2_{SN} to describe the supernovae Ia data [3].

This approach with separation of the Hubble constant H_0 among other model parameters can not be applied to $H(z)$ and BAO observational data, because observed values have different dependence on H_0.

To describe the BAO data we calculate the distance [5, 8–10]

$$D_V(z) = \left[\frac{czD_L^2(z)}{(1+z)^2 H(z)}\right]^{1/3}, \tag{6}$$

and two measured values

$$d_z(z) = \frac{r_s(z_d)}{D_V(z)}, \qquad A(z) = \frac{H_0\sqrt{\Omega_m}}{cz} D_V(z), \tag{7}$$

which are usually considered as observational manifestations of baryon acoustic oscillations [5, 8]. Here $\Omega_m = \frac{8}{3}\pi G\rho(t_0)/H_0^2$ is the present time fraction of matter with density ρ. The value $r_s(z_d)$ in Eq. (7) is sound horizon size at the end of the drag era z_d:

$$r_s(z_d) = \int_{z_d}^{\infty} \frac{c_s(z)}{H(z)} dz, \tag{8}$$

To estimate this important parameter different authors [17–33] used theoretical or statistical approaches and suggested different fitting formulas for r_s. In table I the following recent estimations of $r_s(z_d) \equiv r_d$ and $r_d h$ are shown:

Refs	[25]	[9, 24]	[10]	[32]	[33]	[22]	[29]	[18]	[21]	[27, 28, 31]	[26]
$r_s(z_d)$	147.4	147.49	147.6	148.6	148.69	149.28	152.40	152.76	153.19	153.2	153.5
$r_d \cdot h$	98.79	99.26	100.09	99.78	99.62	104.49	105.15	106.93	107.23	103.6	104.69

TABLE I: Recent estimations of $r_s(z_d)$ and $r_s(z_d) \cdot h$ (Mpc).

In the most of cited papers in table I the values $r_s(z_d)$ were considered as fiducial ones for calculating $D_V(z)$, $H(z)$ and other parameters. So these results sufficiently depend on $r_s(z_d)$, in

particular, estimations of $H(z)$ from the BAO data [16–25] are defined with the factor r_d^{fid}/r_d, the corresponding factor r_d/r_d^{fid} takes place for calculated values $D_V(z)$ or $D_A(z) = D_L(z)/(1+z)^2$.

In this paper we use two different approaches to calculate the sound horizon scale $r_s(z_d)$. But previously one should mention the simplest method, applied in Ref. [39], where the arithmetic average of the r_d values in table I (with their multiplicity)

$$r_s(z_d) = 150.69 \pm 2.45 \text{ Mpc} \tag{9}$$

was used as the basic value. This value is independent on H_0, hence the observational parameter $d_z(z)$ in Eq. (7) appears to be Hubble dependent (though the formula (8) predicts $r_d \sim H_0^{-1}$ and Hubble free d_z). One may conclude, that h dependence of d_z is the drawback of this approach, so in this paper we consider the fixed value r_d (9) only in section III to emphasize advantages of other methods.

More appropriate procedures to calculate $r_s(z_d)$ include different fitting formulae [6, 7, 22, 57]. In this paper we use the numerically calibrated approximation from Ref. [7]

$$r_s(z_d) = \frac{55.154 \exp\left[72.3(\Omega_\nu h^2 + 0.0006)^2\right]}{(\Omega_m h^2)^{0.25351}(\Omega_b h^2)^{0.12807}} \text{ Mpc} \tag{10}$$

as the basic formula. The resulting h dependence in Eq. (10) (for a reasonable neutrino contribution with $\sum m_\nu \leq 0.23$ eV [10]) is $r_d \sim h^{-0.7632}$, it is more close to the true variant $r_d \sim h^{-1}$. The dependence on Ω_m in Eq. (10) is well fitted for ΛCDM-like models, however for the models with Chaplygin gas and with quadratic EoS, considered below, Ω_m is not a basic model parameter. The value Ω_m in these models should be estimated in a special way, so an additional uncertainty appears in this approach.

Thus, an alternative simple fitting formula

$$r_s(z_d) = \frac{(r_d \cdot h)_{fid}}{h}, \qquad (r_d \cdot h)_{fid} = 104.57 \text{ Mpc}. \tag{11}$$

with true h dependence may be suggested. Here the value $(r_d \cdot h)_{fid} = 104.57 \pm 1.44$ Mpc was chosen as the best fit for the ΛCDM model. This procedure is described in the next section and illustrated in figure 1.

The parameter $(r_d \cdot h)_{fid}$ for the expression (11) plays the same role as the baryonic fraction Ω_b for the formula (10), in both cases we do not consider Ω_b and $r_d h$ as free model parameters for all models, but fix their optimal (fiducial) values after description of the simplest ΛCDM model. The best ΛCDM fit for Ω_b in Eq. (10) (see figure 1) is

$$\Omega_b = 0.044 \pm 0.004. \tag{12}$$

To take into account all available BAO data [16–33] for parameters (7), we consider in this paper $N_{BAO} = 17$ data points for $d_z(z)$ (10 additional points in comparison with the table in our paper [39]) and 7 data points for $A(z)$ presented in the table II.

Measurements of $d_z(z)$ and $A(z)$ from Refs. [26, 29] in table II are not independent. So the χ^2 function for the values (7) is

$$\chi^2_{BAO}(p_1, p_2, \ldots) = (\Delta d)^T C_d^{-1} \Delta d + (\Delta A)^T C_A^{-1} \Delta A, \qquad \Delta d = d_z(z_i) - d_z^{th}. \tag{13}$$

The elements of covariance matrices $C_d^{-1} = ||c_{ij}^d||$ and $C_A^{-1} = ||c_{ij}^A||$ in Eq. (13) are [8, 26, 29]:

$$\begin{array}{llll} c_{33}^d = 30124, & c_{38}^d = -17227, & c_{88}^d = 86977, & \\ c_{11\,11}^d = 24532.1, & c_{11\,14}^d = -25137.7, & c_{11\,15}^d = 12099.1, & c_{14\,14}^d = 134598.4, \\ c_{14\,15}^d = -64783.9, & c_{15\,15}^d = 128837.6; & c_{11\,11}^A = 1040.3, & c_{11\,14}^A = -807.5, \\ c_{11\,15}^A = 336.8, & c_{14\,14}^A = 3720.3, & c_{14\,15}^A = -1551.9, & c_{15\,15}^A = 2914.9. \end{array}$$

z	$d_z(z)$	σ_d	$A(z)$	σ_A	Refs	Survey
0.106	0.336	0.015	0.526	0.028	[8, 28]	6dFGS
0.15	0.2232	0.0084	-	-	[33]	SDSS DR7
0.20	0.1905	0.0061	0.488	0.016	[26, 29]	SDSS DR7
0.275	0.1390	0.0037	-	-	[26]	SDSS DR7
0.278	0.1394	0.0049	-	-	[27]	SDSS DR7
0.314	0.1239	0.0033	-	-	[29]	SDSS LRG
0.32	0.1181	0.0026	-	-	[22]	BOSS DR11
0.35	0.1097	0.0036	0.484	0.016	[26, 29]	SDSS DR7
0.35	0.1126	0.0022	-	-	[30]	SDSS DR7
0.35	0.1161	0.0146	-	-	[19]	SDSS DR7
0.44	0.0916	0.0071	0.474	0.034	[29]	WiggleZ
0.57	0.0739	0.0043	0.436	0.017	[20]	SDSS DR9
0.57	0.0726	0.0014	-	-	[22]	SDSS DR11
0.60	0.0726	0.0034	0.442	0.020	[29]	WiggleZ
0.73	0.0592	0.0032	0.424	0.021	[29]	WiggleZ
2.34	0.0320	0.0021	-	-	[25]	BOSS DR11
2.36	0.0329	0.0017	-	-	[24]	BOSS DR11

TABLE II: Values of $d_z(z) = r_s(z_d)/D_V(z)$ and $A(z)$ (7) with errors and references

Here $c_{ij} = c_{ji}$, the remaining matrix elements are $c_{ii} = 1/\sigma_i^2$, $c_{ij} = 0$, $i \neq j$.

In the values σ_d in table II we took into account correlation between estimations of $d_z(z)$ and $H(z)$ (table III) for $z = 0.35$, 0.57, 2.34, 2.36 in Refs. [19–21, 24, 25].

Measurements of the Hubble parameter $H(z)$ for different redshifts z with 38 data points [11–25] are presented in table III. These values $H(z)$ were calculated with two methods: 1) differential age approach in Refs. [11–15] with evaluation of the age difference dt for galaxies with close redshifts dz and the formula

$$H(z) = \frac{1}{a(t)}\frac{da}{dt} = -\frac{1}{1+z}\frac{dz}{dt},$$

2) measurement [16–25] of the BAO peak in the correlation function in line-of-sight directions at a redshift separation $\Delta z = r_s(z_d)\, H(z)/c$.

For the latter method estimations [16–25] of $H(z)$ essentially depend on a fiducial value r_d^{fid} and have the factor r_d^{fid}/r_d, as was mentioned above. In particular, the result in Ref. [25] is

$$H(z = 2.34) = (222 \pm 7)\,\frac{\mathrm{km}}{\mathrm{s}\cdot\mathrm{Mpc}} \cdot \frac{147.4\ \mathrm{Mpc}}{r_s(z_d)}.$$

In table III this factor is taken into account only for the errors σ_H from the papers [16, 18–20, 24, 25], where fiducial values r_d^{fid} essentially differ from the average (9). The estimations for $H(z)$ in table III are the same as in the correspondent sources.

To compare the $H(z)$ data in table III with $N_H = 38$ data points with model predictions we use the χ^2 function

$$\chi^2_H(p_1, p_2, \ldots) = \sum_{i=1}^{N_H} \frac{\left[H_i - H^{th}(z_i, p_1, p_2, \ldots)\right]^2}{\sigma^2_{H,i}}, \tag{14}$$

similar to the function (3) for the SN Ia observational data from Ref. [3].

z	$H(z)$	σ_H	Refs	z	$H(z)$	σ_H	Refs
0.070	69	19.6	[14]	0.570	96.8	3.4	[22]
0.090	69	12	[11]	0.593	104	13	[13]
0.120	68.6	26.2	[14]	0.600	87.9	6.1	[17]
0.170	83	8	[11]	0.680	92	8	[13]
0.179	75	4	[13]	0.730	97.3	7.0	[17]
0.199	75	5	[13]	0.781	105	12	[13]
0.200	72.9	29.6	[14]	0.875	125	17	[13]
0.240	79.69	2.99	[16]	0.880	90	40	[12]
0.270	77	14	[11]	0.900	117	23	[11]
0.280	88.8	36.6	[14]	1.037	154	20	[13]
0.300	81.7	6.22	[23]	1.300	168	17	[11]
0.340	83.8	3.66	[16]	1.363	160	33.6	[15]
0.350	82.7	9.1	[19]	1.430	177	18	[11]
0.352	83	14	[13]	1.530	140	14	[11]
0.400	95	17	[11]	1.750	202	40	[11]
0.430	86.45	3.97	[16]	1.965	186.5	50.4	[15]
0.440	82.6	7.8	[17]	2.300	224	8.6	[18]
0.480	97	62	[12]	2.340	222	8.5	[25]
0.570	87.6	7.8	[20]	2.360	226	9.3	[24]

TABLE III: Values of the Hubble parameter $H(z)$ with errors σ_H from Refs. [11–25]

We mentioned above that the observed values in tables II, III have different dependence on $h = H_0/100\ \mathrm{km\,s^{-1}Mpc^{-1}}$. In particular, if we use the fitting formula (10) for $r_s(z_d)$, the parameter d_z (7) has rather weak h dependence ($d_z \sim h^{0.2368}$, because $D_V \sim h^{-1}$); for the formula (11) d_z is Hubble free in accordance with Eq. (7). The value $A(z)$ is also Hubble free, but it depends on Ω_m. The values $H(z)$ in table III are naturally proportional to H_0. So estimations in tables II, III may be model dependent, but we can assume that different authors use different methods and produce possible systematic errors for $d_z(z)$ and $H(z)$ in different directions. One can suppose mean systematic errors to be close to zero.

On the other hand, if any form of marginalization over H_0 for BAO and $H(z)$ data is made [55–57], the obtained results will have an additional error, because a model can successfully describe all SN Ia, BAO and $H(z)$ data, but with 3 essentially different intrinsic values of H_0. Under these arguments we make the marginalization procedure (5) over H_0 only for SN Ia data [3], but not for BAO and $H(z)$ data from tables II, III.

III. ΛCDM MODEL

In the ΛCDM and other models in this paper the Einstein equations

$$G^\mu_\nu = 8\pi G T^\mu_\nu - \Lambda \delta^\mu_\nu \tag{15}$$

describe dynamics of the universe. Here $G^\mu_\nu = R^\mu_\nu - \frac{1}{2}R\delta^\mu_\nu$, $T^\mu_\nu = \mathrm{diag}\,(-\rho, p, p, p)$.

In the ΛCDM model baryonic and dark matter may be described as one component of dust-like matter with density $\rho = \rho_c = \rho_b + \rho_{dm}$, so we suppose $p = 0$ in T^μ_ν. In models with Chaplygin gas (Sect. IV) and with quadratic equation of state (Sect. V) we suppose that an additional component of matter describes both dark matter and dark energy and gives some contribution ρ_g in the total

density:

$$\rho = \rho_c + \rho_g + \rho_r. \tag{16}$$

The fraction of relativistic matter (radiation and neutrinos) is close to zero for observable values $z \leq 2.36$, so below we suppose $\rho_r = 0$.

For the Robertson-Walker metric with the curvature sign k

$$ds^2 = -dt^2 + a^2(t)\Big[(1-kr^2)^{-1}dr^2 + r^2 d\Omega\Big] \tag{17}$$

the Einstein equations (15) are reduced to the system

$$3\frac{\dot{a}^2 + k}{a^2} = 8\pi G\rho + \Lambda, \tag{18}$$

$$\dot{\rho} = -3\frac{\dot{a}}{a}(\rho + p). \tag{19}$$

Eq. (19) results from the continuity condition $T^{\mu}_{\nu;\mu} = 0$, the dot denotes the time derivative, here and below the speed of light $c = 1$.

For the ΛCDM with dust-like matter ($p = 0$) we use the solution of Eq. (19) $\rho/\rho_0 = (a/a_0)^{-3}$ and rewrite Eq. (18) in the form

$$\frac{\dot{a}^2}{a^2 H_0^2} = \frac{H^2}{H_0^2} = \Omega_m\Big(\frac{a}{a_0}\Big)^{-3} + \Omega_\Lambda + \Omega_k\Big(\frac{a}{a_0}\Big)^{-2}. \tag{20}$$

Here the present time fractions of matter, dark energy (Λ term) and curvature

$$\Omega_m = \frac{8\pi G\rho(t_0)}{3H_0^2}, \qquad \Omega_\Lambda = \frac{\Lambda}{3H_0^2}, \qquad \Omega_k = -\frac{k}{a_0^2 H_0^2} \tag{21}$$

are connected by the equality

$$\Omega_m + \Omega_\Lambda + \Omega_k = 1, \tag{22}$$

resulting from Eq. (20) if we fix $t = t_0$.

If we introduce dimensionless time τ and logarithm of the scale factor [38]

$$\tau = H_0 t, \qquad \mathcal{A} = \log\frac{a}{a_0}. \tag{23}$$

equation (20) will take the form $\frac{d\mathcal{A}}{d\tau} = \sqrt{\Omega_m e^{-3\mathcal{A}} + \Omega_\Lambda + \Omega_k e^{-2\mathcal{A}}}$, more convenient for numerical solving with the initial condition at the present time $\mathcal{A}|_{\tau=1} = 0$ equivalent to $a(t_0) = a_0$. Here and below the present time $t = t_0$ corresponds to $\tau = 1$.

If we fix all model parameters, we can solve numerically the Cauchy problem for Eq. (20) and calculate the values $a(t)/a_0$, $H(z)$, $D_L(z)$ (1), $d_z(z)$ and $A(z)$ (7). To compare them with the observational data from Ref. [3] and tables II, III we use the χ^2 functions (3), (13) and (14) and (under assumption about their Gaussian nature) the correspondent summarized function

$$\chi^2_\Sigma = \chi^2_{SN} + \chi^2_H + \chi^2_{BAO}. \tag{24}$$

When we apply the ΛCDM model for describing the observational data from Sect. II (for $z \leq 2.36$), we use three free model parameters H_0, Ω_m and Ω_Λ (or Ω_k instead of Ω_Λ) and the additional parameter

$$\Omega_b = \frac{\rho_b(t_0)}{\rho_{cr}} = \frac{8\pi G\rho_b(t_0)}{3H_0^2}, \tag{25}$$

if we use the fitting formula (10) for $r_s(z_d)$. For the formula (11) the baryonic fraction Ω_b is not a model parameter, we mentioned above that the value $r_d \cdot h$ plays the role of an additional parameter in the case (11). In both approaches we test the ΛCDM model and estimate the best ΛCDM fit correspondingly for Ω_b and $r_d \cdot h$.

The results are presented in figure 1, where dependence of the best (minimal) value of the function (24) $\min \chi^2_\Sigma = \min\limits_{H_0,\Omega_m,\Omega_\Lambda} \chi^2_\Sigma$ on Ω_b is shown in the top-left panel for the case (10). Here and for all models we assume $\sum m_\nu = 0.06$ eV [7, 9]. One should note that the formula (10) is insensitive to a neutrino contribution in the range $\sum m_\nu \leq 0.23$ eV [10].

For the variant with Eq. (11) the similar dependence of $\min \chi^2_\Sigma$ on $r_d \cdot h$ is in the top-right panel. Here and below we draw these graphs as solid red lines for the fitting formula (10) and as dashed blue lines for the variant (11).

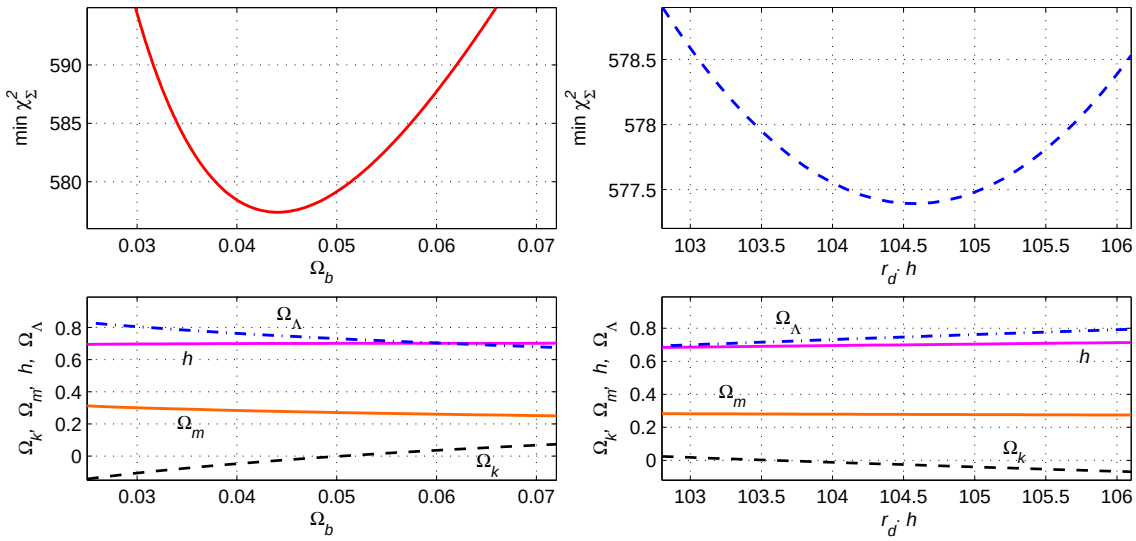

FIG. 1: The ΛCDM model: dependence of the best fit $\min\limits_{H_0,\Omega_m,\Omega_\Lambda} \chi^2_\Sigma$ on Ω_b for the fitting formula (10) (the left panels) and on $r_d \cdot h$ for Eq. (11) (the right panels). In the bottom panels we show the correspondent dependencies for parameters H_0, Ω_m, Ω_Λ, Ω_k of the χ^2_Σ minimum point.

The bottom panels of figure 1 illustrate how coordinates h, Ω_m, Ω_Λ and $\Omega_k = 1 - \Omega_m - \Omega_\Lambda$ of the minimum point for $\min\limits_{H_0,\Omega_m,\Omega_\Lambda} \chi^2_\Sigma$ depend on the correspondent parameters Ω_b and $r_d \cdot h$.

One can see that for the formula (10) dependence of $\min \chi^2_\Sigma$ on Ω_b is rather sharp: we have the distinct minimum at the value (12) $\Omega_b = 0.044$. Below we use this value as the fiducial one for all models. The correspondent dependence in the top-right panel is more smooth, however it results in the optimal (fiducial) value $r_d \cdot h = 104.57 \pm 1.44$ Mpc in the formula (11).

If we fix these parameters as described above, we can test the ΛCDM model for different values of the remaining 3 parameters: H_0, Ω_m and Ω_Λ. The results of calculations are presented in tables IV, V, VI and in figure 2. In the top-left panel of the figure we see how minimum of the function (24) $\min \chi^2_\Sigma = \min\limits_{\Omega_m,\Omega_\Lambda} \chi^2_\Sigma(H_0)$ depend on the Hubble constant H_0: red solid lines in the top panels describe the model with the formula (10), blue dashed lines correspond to the variant (11). For the sake of comparison we present here graphs for the fixed value $r_s(z_d)$ (9) as green lines with dots. These minima are calculated for each fixed value H_0.

One may see that the function $\min \chi^2_\Sigma(H_0)$ for the fitting formula (10) (the red line) has the maximal spread and achieves its minimum $\min \chi^2_\Sigma \simeq 577.39$ at

$$H_0 = 70.07 \pm 1.82 \quad \text{km}\,(\text{s}\,\text{Mpc})^{-1} \tag{26}$$

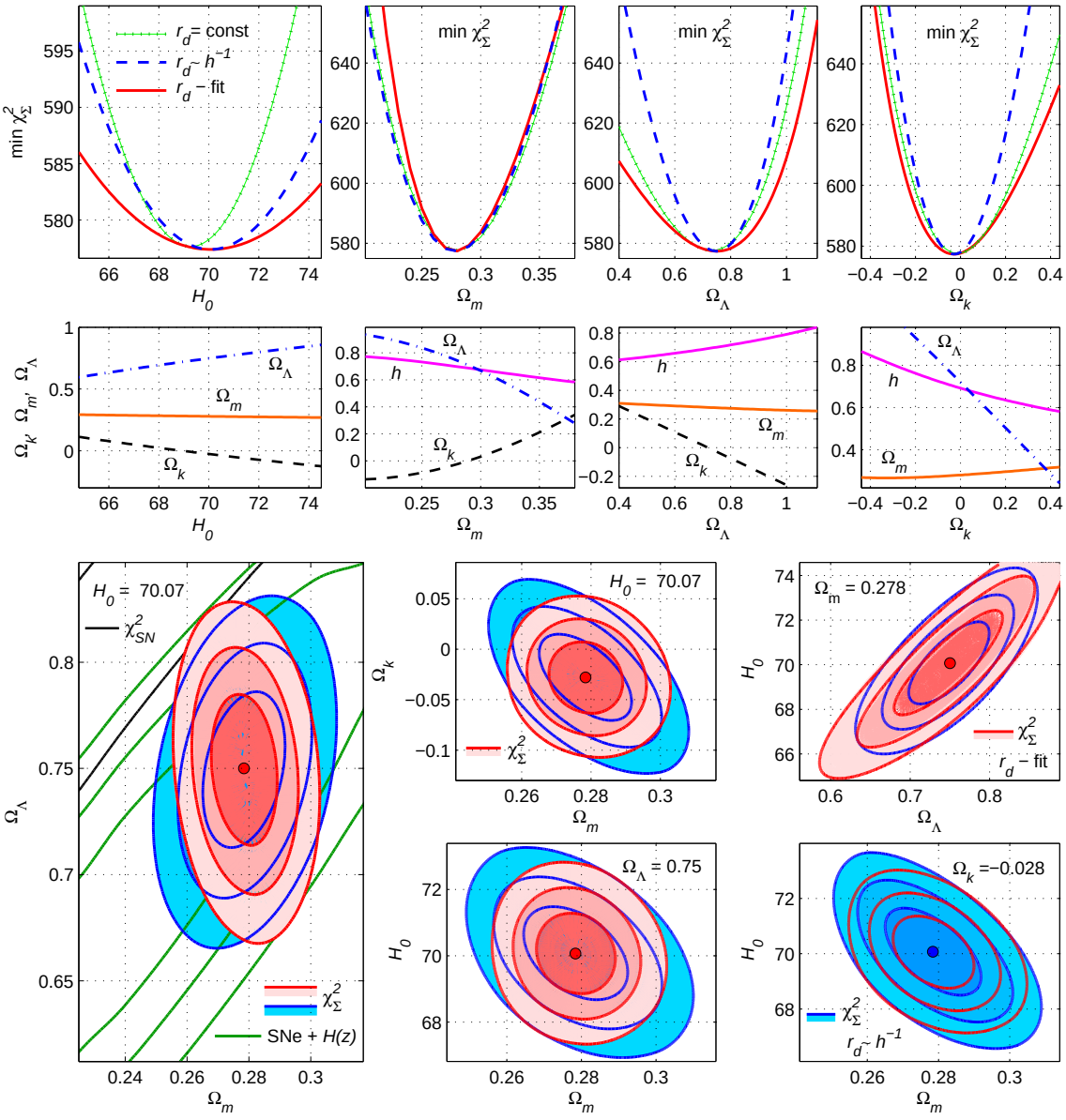

FIG. 2: For the ΛCDM in the top panels we present how $\min\chi^2_\Sigma$ depends on H_0, Ω_m, Ω_Λ and Ω_k with different fitting formulae for r_d: for Eq. (10) with $\Omega_b = 0.044$ (red solid lines), for Eq. (11) (blue dashed lines), for Eq. (9) (green lines with dots). The correspondent dependencies for parameters of χ^2_Σ minimum point for Eq. (10) are shown in the 2-nd row. In other panels 1σ, 2σ and 3σ level lines are drawn for χ^2_Σ as red filled contours for Eq. (10) and blue filled contours for Eq. (11) and also as black lines for χ^2_{SN} and green lines for $\chi^2_{SN} + \chi^2_H$; optimal values of the third parameter are fixed and shown.

for the following values of other parameters: $\Omega_m \simeq 0.278$, $\Omega_\Lambda \simeq 0.75$ (presented in table IV). It is interesting to see in table IV and in figure 2 that for the fitting formula (11) (blue dashed lines) the minimum $\min\chi^2_\Sigma$ and the optimal values of all parameters are the same, there is some difference only in 1σ errors. To estimate 1σ errors in the equality (26) we use the one-dimensional likelihood function $\mathcal{L}_\Sigma(H_0) \sim \exp(-\chi^2_\Sigma/2)$ corresponding to $\min\limits_{\Omega_m,\Omega_\Lambda} \chi^2_\Sigma(H_0)$.

Optimal values and errors for other model parameters Ω_m, Ω_Λ, Ω_k are calculated similarly, they are tabulated below in table IV in comparison with other estimates and also in the next section in

tables V and VI correspondingly for the expressions (10) and (11).

Estimations of Ω_m and Ω_Λ in tables IV, V, VI are connected with graphs in the next two panels in the top line of figure 2, which present how minima of χ^2_Σ depend on Ω_m and on Ω_Λ. In particular, the solid red line in the second top panel describes $\min\chi^2_\Sigma(\Omega_m) = \min\limits_{H_0,\Omega_\Lambda}\chi^2_\Sigma$; the corresponding likelihood function $\mathcal{L}_\Sigma(\Omega_m) \sim \exp(-\chi^2_\Sigma/2)$ determines the 1σ error $\Delta\Omega_m \simeq 0.008$ in tables IV, V. This panel demonstrates that dependencies of $\min\chi^2_\Sigma$ on Ω_m for different variants of $r_s(z_d)$ are rather close and have rather sharp form. It is connected with the contribution in χ^2_{BAO} from the value $A(z)$ (7), because $A(z)$ is proportional to $\sqrt{\Omega_m}$ and χ^2_{BAO} is very sensitive to Ω_m values. For the red line in this panel we have the additional dependence on Ω_m in the formula (10). In the third panel the functions $\min\chi^2_\Sigma(\Omega_\Lambda)$ with distinct minima have some difference in their the 1σ errors.

Estimations of Ω_k in tables IV – VI are calculated via the function $\min\chi^2_\Sigma(\Omega_k) = \min\limits_{H_0,\Omega_m}\chi^2_\Sigma$. These graphs are shown in the top-right panel of figure 2.

The panels in the second row in figure 2 demonstrate how parameters of a minimum point of the function χ^2_Σ with the fitting formula (10) depend on H_0, Ω_m, Ω_Λ, Ω_k. In the left panel these coordinates are Ω_m and Ω_Λ, but also the value $\Omega_k = 1-\Omega_m-\Omega_\Lambda$ is drawn as the black dashed line. The optimal value Ω_m remains practically constant in contrast with Ω_Λ and Ω_k. The graphs of $h(\Omega_m),\ldots,h(\Omega_k)$ in other panels show $h = H_0/100$, where H_0 is the optimal value corresponding to the minimum point of χ^2_Σ.

In other panels of figure 2 we present the results of calculations as level lines at 1σ (68.27%), 2σ (95.45%) and 3σ (99.73%) confidence levels for the functions $\chi^2(p_1,p_2)$ in planes of two parameters, if the third parameter is fixed. For example, the functions $\chi^2_\Sigma(\Omega_m,\Omega_\Lambda)$ for the fixed optimal value (26) of H_0 are shown in the bottom-left panel of figure 2 as red filled contours for the formula (10) and blue filled contours for Eq. (11). The corresponding level lines for χ^2_{SN} and for $\chi^2_{SN}+\chi^2_H$ are shown as black and green lines.

In other panels only χ^2_Σ filled contours for the cases (10) and (11) are compared for different pairs of parameters. Points of minima for the functions χ^2_Σ are marked as red (or blue) circles, we mentioned above, that they coincide for the variants (10) and (11). In two bottom-left panels the difference is in the fixed parameter (Ω_Λ or Ω_k) and in a choice of the foreground between the cases (10) and (11).

Our estimations of the ΛCDM parameters for two variants (10) and (11) of the fitting formula for r_d are to be compared with the the following best fits for these model parameters from surveys of the Wilkinson Microwave Anisotropy Probe (WMAP) [8] and Planck Collaboration [9, 10] in table IV.

	This paper		WMAP, Planck surveys		
	r_d (10)	r_d (11)	WMAP 9y [8]	Planck 13 [9]	Planck 15 [10]
H_0	70.07 ± 1.82	70.07 ± 1.27	69.7 ± 2.4	67.3 ± 1.2	67.8 ± 0.9
Ω_m	0.278 ± 0.008	0.278 ± 0.009	0.279 ± 0.025	0.314 ± 0.02	0.308 ± 0.012
Ω_Λ	$0.750^{+0.051}_{-0.055}$	0.750 ± 0.034	0.721 ± 0.025	0.686 ± 0.025	0.692 ± 0.012
Ω_k	$-0.028^{+0.050}_{-0.048}$	$-0.028^{+0.035}_{-0.034}$	$-0.0027^{+0.0039}_{-0.0038}$	$-0.0005^{+0.0065}_{-0.0066}$	$-0.005^{+0.016}_{-0.017}$
Ω_b	0.044 ± 0.004	-	$0.0463^{+0.0024}_{-0.0024}$	$0.0487^{+0.0018}_{-0.0017}$	$0.0484^{+0.0014}_{-0.0013}$

TABLE IV: Estimations of the ΛCDM parameters.

One can also add the estimates for the fixed r_d (9): $H_0 = 69.27 \pm 0.93$ km s^{-1}Mpc^{-1}, $\Omega_m = 0.280 \pm 0.009$, $\Omega_\Lambda = 0.732^{+0.044}_{-0.055}$, $\Omega_k = -0.012 \pm 0.045$ (corresponding to green dots in the top panels in figure 2). In the case (9) the 1σ error for H_0 is smallest, because d_z^{th} depends on h.

We see that our estimations of the model parameters in table IV for the cases (10) and (11) are in good agreement with the WMAP estimates, but they are in 1σ or 2σ tension with the values of Planck Collaboration. On the other hand, all H_0 values in table IV have essential tension with the Hubble Space Telescope group [58] estimation: $H_0 = 73.8 \pm 2.4$ km s^{-1}Mpc^{-1}.

The latter value was used as a prior in Refs. [55, 56] for describing Type Ia SNe, BAO and $H(z)$ data with the help of the ΛCDM, XCDM and ϕCDM models. One may conclude, that for the ΛCDM this choice of H_0 was unsuccessful in comparison with another value $H_0 = 68$ km s^{-1}Mpc^{-1}, chosen in Refs. [55, 56].

IV. MODIFIED CHAPLYGIN GAS

In the model with modified Chaplygin gas (MCG) this gas has the following equation of state [41–47]

$$p_g = w_0\rho_g - B\,\rho_g^{-\alpha} \tag{27}$$

for its density ρ_g as a part in the total density (16). MCG can unify dark matter and dark energy. If $w_0 = 0$ the MCG model with Eq. (27) is reduced to the model with generalized Chaplygin gas (GCG) with EoS [40, 59]

$$p_g = -B\,\rho_g^{-\alpha}. \tag{28}$$

In our paper [39] the GCG model was applied to describing the observational data for Type Ia supernovae [3], $H(z)$ with 34 data points and BAO with 7 data points for $d_z(z)$. In this paper we consider the enlarged number of data points from tables II, III, the more general MCG model (27) (in comparison with the GCG case $w_0 = 0$) and also we calculate the function χ^2_{SN} (3) with the covariance matrix C_{SN}.

The MCG and GCG models are to be explored as two-component models with usual dust-like baryonic matter component ρ_b and the Chaplygin gas component ρ_g with EoS (27). In this case the total density (16) is

$$\rho = \rho_b + \rho_g, \qquad p_b = 0. \tag{29}$$

However the first component ρ_b and the corresponding fraction Ω_b (25) may include not only visible baryonic matter but also a part of cold dark matter with $\rho = \rho_{dm}$. Our practical applications of these models in Ref. [39] and in this paper (see the top-right panel of figure 3) demonstrate rather weak dependence of $\min\chi^2_\Sigma$ on Ω_b for the model assumption (11), but the strong Ω_b dependence for the fitting formula (10). This behavior resembles the ΛCDM model, where separation of baryonic and cold dark matter in Ω_m appears only in Eq. (10). In the MCG and GCG models these matter fractions may also be mixed in their observational manifestations, so below we did not use Ω_b as an usual free parameter of the theory, but fix its fiducial value (12) in the main part this research (except for calculations, presented in right panels if figures 3 and 4).

Equation (19) for the MCG model (27) is integrable, so the analog of Eq. (20) for this model is [41–47]

$$\frac{H^2}{H_0^2} = \Omega_b\Big(\frac{a}{a_0}\Big)^{-3} + \Omega_k\Big(\frac{a}{a_0}\Big)^{-2} + (1-\Omega_b-\Omega_k)\Big[B_s + (1-B_s)\Big(\frac{a}{a_0}\Big)^{-3(1+w_0)(1+\alpha)}\Big]^{1/(1+\alpha)}. \tag{30}$$

Here the dimensionless parameter $B_s = B\rho_0^{-1-\alpha}/(1+w_0)$ is used instead of B. Thus in the MCG model (27) we have 6 independent parameters: H_0, Ω_b, Ω_k, w_0, α and B_s. Naturally, the GCG model has 5 parameters: the same set without w_0.

In the MCG model the parameter Ω_m from its formal definition (21) equals $\Omega_m = 1 - \Omega_k$ in accordance with $\Omega_\Lambda = 0$ and Eq. (22). However, the expression $A(z)$ (7) has the factor $\sqrt{\Omega_m}$, so one should use the effective value Ω_m^{eff} in any model. If we compare the early universe limit $z \gg 1$ in the MCG equation (30) with the ΛCDM equation (20), we obtain the effective value [45–47]:

$$\Omega_m^{eff} = \Omega_b + (1 - \Omega_b - \Omega_k)(1 - B_s)^{1/(1+\alpha)}. \tag{31}$$

But for the majority of observational data in Ref. [3] and tables II, III redshifts are $0 < z < 1$, so to describe correctly these data we have to consider the present time limit of Eq. (30). If we compare limits of the right hand sides of Eqs. (20) and (30) at $z \to 0$ or $\mathcal{A} \to 0$, we obtain another effective value [39]

$$\Omega_m^{eff} = \Omega_b + (1 - \Omega_b - \Omega_k)(1 - B_s)(1 + w_0). \tag{32}$$

Expressions (31) and (32) and their contributions in χ^2_{BAO} and χ^2_Σ were compared in Ref. [39]. In this paper we use below Eq. (32) and its analogs for other models.

Figure 3 shows how the MCG model (27) describes the observational data from Ref. [3] and tables II, III in comparison with the GCG model (28). Notations are the same as in figure 2. In the top line panels red solid lines and blue dashed lines denote graphs of $\min \chi^2_\Sigma$ for the MCG model with expressions (10) and (11) correspondingly. The similar functions for the GCG model are shown as orange dash-dotted lines, if $r_s(z_d)$ is calculated with the formula (10) and as violet dashed lines for the case (11).

These graphs in the top line describe how χ^2_Σ for the mentioned models depends on one chosen model parameter: H_0, Ω_k, w_0, α, Ω_b. All these curves determine the optimal values and errors of the model parameters in tables V, VI. The second row panels of figure 3 correspond to panels in the top line and present dependencies of coordinates of minima points on $H_0, \ldots, \Omega_b$ for χ^2_Σ in the MCG model with the fitting formula (10).

In the top-right panel of figure 3 the value $\min \chi^2_\Sigma$ for the MCG model means the minimum over other 5 parameters for each fixed Ω_b: $\min \chi^2_\Sigma = \min\limits_{H_0,\Omega_k,w_0,\alpha,B_s} \chi^2_\Sigma$. Our calculations support the previous conclusion [39] about weak dependence of $\min \chi^2_\Sigma$ on Ω_b for the case (11) with $r_d = (r_d h)_{fid} \cdot h^{-1}$ as for the the fixed value r_d (9) for both models. This is connected with possible mixing of baryonic and cold dark matter in Ω_b. However, for and the fitting formula (10) we see the sharp dependence of $\min \chi^2_\Sigma$ on Ω_b; for both MCG and GCG models this picture coincides with behavior of the ΛCDM model in figure 1. As mentioned above, we will not use Ω_b as an usual free model parameter and we fix its ΛCDM fiducial value (12). It is interesting that for the MCG and GCG models this value $\Omega_b \simeq 0.044 \pm 0.004$ is very close and practically coincides with the ΛCDM fiducial value of this parameter.

In figure 3 the parameter Ω_b is varied only in 3 right panels, in other 12 panels this value is fixed in the form (12). In particular, the value $\min \chi^2_\Sigma(H_0)$ for the MCG model in the top-left panel is the minimum over 4 parameters $\min\limits_{\Omega_k,w_0,\alpha,B_s} \chi^2_\Sigma$ with fixed $\Omega_b = 0.044$. The similar picture takes place, when we study dependence of these minimal functions on Ω_k, w_0, α, for example, $\min \chi^2_\Sigma(\Omega_k) = \min\limits_{H_0,w_0,\alpha,B_s} \chi^2_\Sigma$. For the GCG model with $w_0 = 0$ these minima (orange dash-dotted lines and violet dashed lines) are taken over 3 remaining parameters.

The graphs of $\min \chi^2_\Sigma(H_0)$ in the top-left panel with two expressions for $r_s(z_d)$ resemble the ΛCDM case in figure 2 for both MCG and GCG models. For all three considered models this curve for the case (11) is slightly more sharp than for the formula (10), this behavior may be seen in tables V, VI, where all models are compared. Unlike the ΛCDM model, for the MCG and GCG models we have different optimal values of H_0 (and also of Ω_k, α and other parameters) in the cases (10) and (11).

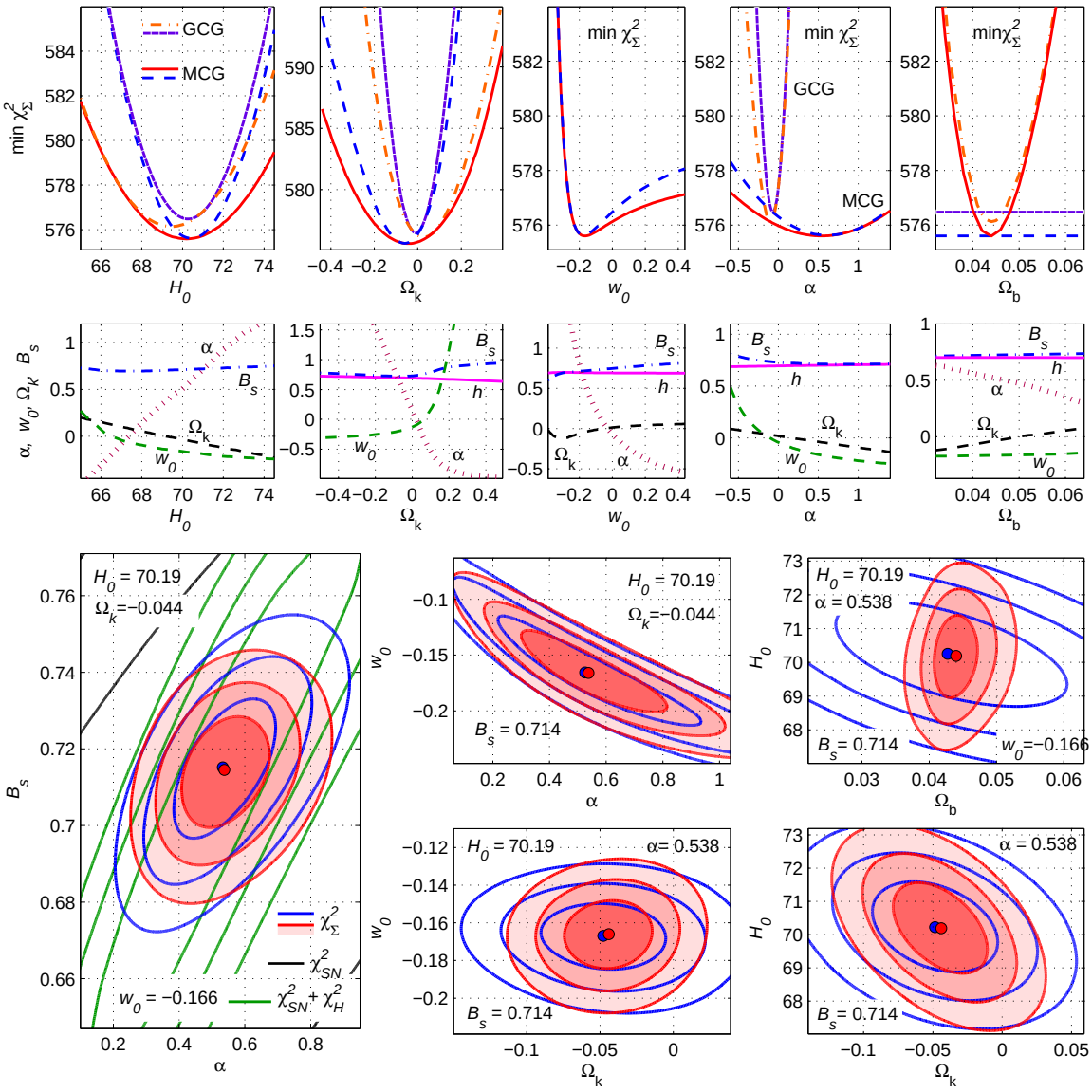

FIG. 3: For the MCG model dependencies of $\min\chi^2_\Sigma$ on one chosen parameter H_0, Ω_k, w_0, α, Ω_b are presented for the fitting formulae (10) (red solid lines) and (11) (blue dashed lines) in comparison with the GCG model (orange dash-dotted lines and violet dashed lines for these two choices of r_d). In the second row there are correspondent MCG parameters of a minimum point for χ^2_Σ with Eq. (10). In other panels for the MCG model 1σ, 2σ, 3σ level lines are drawn in the planes of 2 parameters (other parameters are fixed). Notations correspond to figure 2.

Obviously that for the GCG model the graphs of χ^2_Σ in the top panels of figure 3 lie higher, then the correspondent MCG graphs. These curves converge at points, where the optimal value of w_0 equals zero in the panel below.

The graphs of $\min\chi^2_\Sigma(\Omega_k)$ in the second top panel are asymmetric, for $\Omega_k > 0$ these values for the GCG and MCG models are close, but for $\Omega_k < 0$ the curves for these models diverge for both variants of $r_s(z_d)$. In the third top panel we have asymmetric dependence of these minima on w_0 for the MCG model.

Dependence od $\min\chi^2_\Sigma$ on α is essentially different for the considered models: for the GCG model these curves have sharp minima, in particular, for the case (10) at $\alpha \simeq -0.1$ with $\sigma \simeq 0.1$,

but for the MCG model the dependence is rather smooth, the minimum at $\alpha \simeq 0.54$ has $\sigma \simeq 0.9$. These results are also presented in table V, correspondent values for the function (11) are in table VI. One may conclude that changes of the parameter w_0 may compensate changes of α.

In 5 bottom panels of figure 3 for the MCG model we present 1σ, 2σ and 3σ level lines in the planes of 2 model parameters (in notations of figure 2), in particular, red filled contours denote levels of χ^2_Σ with the fitting formula (10). For this case in the bottom-left panel in the (α, B_s) plane contours for χ^2_{SN} (black) and $\chi^2_{SN} + \chi^2_H$ (green lines) are also shown. Contours for χ^2_Σ with the formula (11) in all panels are drawn as blue lines. Other model parameters are fixed and shown in the panels and in table V, they are optimal for the fitting formula (10) (but not optimal for the case (11)).

Model	$\min \chi^2_\Sigma$	H_0	Ω_k	other parameters
ΛCDM	577.39	70.07 ± 1.82	$-0.028^{+0.050}_{-0.048}$	$\Omega_m = 0.278 \pm 0.008$, $\Omega_\Lambda = 0.750^{+0.051}_{-0.055}$
GCG	576.13	69.46 ± 1.88	$0.026^{+0.075}_{-0.069}$	$\alpha = -0.100^{+0.090}_{-0.098}$, $B_s = 0.738^{+0.024}_{-0.022}$
MCG	575.60	70.19 ± 2.15	-0.044 ± 0.122	$\alpha = 0.538^{+0.902}_{-0.893}$, $B_s = 0.714^{+0.033}_{-0.031}$, $w_0 = -0.166^{+0.322}_{-0.089}$
EoS (34)	575.15	$70.28^{+2.22}_{-2.10}$	$-0.045^{+0.102}_{-0.094}$	$p_0 = -0.904^{+0.256}_{-0.248}$, $\beta = -0.042^{+0.041}_{-0.038}$, $w_0 = 0.183 \pm 0.222$

TABLE V: Models and 1σ estimates of model parameters, if $r_s(z_d)$ has the form (10); $\Omega_b = 0.044$.

Model	$\min \chi^2_\Sigma$	H_0	Ω_k	other parameters
ΛCDM	577.39	70.07 ± 1.27	$-0.028^{+0.035}_{-0.034}$	$\Omega_m = 0.278 \pm 0.009$, $\Omega_\Lambda = 0.750^{+0.033}_{-0.034}$
GCG	576.48	70.27 ± 1.28	-0.009 ± 0.040	$\alpha = -0.069 \pm 0.074$, $B_s = 0.753 \pm 0.013$
MCG	575.61	70.44 ± 1.30	$-0.060^{+0.068}_{-0.075}$	$\alpha = 0.613^{+0.80}_{-0.744}$, $B_s = 0.716^{+0.058}_{-0.033}$, $w_0 = -0.176^{+0.447}_{-0.078}$
EoS (34)	575.14	70.42 ± 1.30	$-0.048^{+0.054}_{-0.048}$	$p_0 = -0.928^{+0.242}_{-0.230}$, $\beta = -0.045^{+0.043}_{-0.039}$, $w_0 = 0.205^{+0.187}_{-0.180}$

TABLE VI: Models and 1σ estimates of model parameters with $r_s(z_d)$ from Eq. (11); $\Omega_b = 0.044$.

For the GCG model (28) the values in table VI are close to our previous estimations [39] $H_0 = 70.093 \pm 0.369$, $\Omega_k = -0.019 \pm 0.045$, $\alpha = -0.066^{+0.072}_{-0.074}$, $B_s = 0.759^{+0.015}_{-0.016}$ with 7 and 34 data points for $d_z(z)$ and $H(z)$ correspondingly.

These estimates for the MCG model should be compared with similar results for this model in papers [45–47]. The authors of Ref. [45] for the flat model with $\Omega_k = 0$ described the observational data with 557, 15 and 2 data points correspondingly for supernovae, $H(z)$ and BAO, but they also included the cluster X-ray gas mass fraction data. Their 1σ estimations $H_0 = 70.711^{+4.188}_{-3.142}$ and $B_s = 0.7788^{+0.0736}_{-0.0723}$ are more wide then ours in tables V, VI; however $\alpha = 0.1079^{+0.3397}_{-0.2539}$ and the narrow box $w_0 = 0.00189^{+0.00583}_{-0.00756}$ lie inside our 1σ estimates.

In Refs. [46, 47] the MCG model with $\Omega_k = 0$ is applied for describing 12 $H(z)$ data points, 11 points for the growth function $f = d\log\delta/d\log a$ of the large scale structures, 17 points for $\sigma_8(z)$ and also in Ref. [47] observations of supernovae and 1 data point for BAO. The authors did not demonstrate their estimates for H_0, but noted ambiguously "χ^2 function for the background test is minimized by the present Hubble value predicted by WMAP7". The best fit values of other parameters in Ref. [47] are $w_0 = 0.005$, $\alpha = 0.19$, $B_s = 0.825$ with errors, calculated for pairs of these parameters. Only the estimate for B_s is in tension with our results in tables V, VI.

V. MODEL WITH QUADRATIC EQUATION OF STATE

It is interesting to compare the MCG model and the model with quadratic equation of state [48–53]

$$p_g = \tilde{p}_0 + w_0\rho_g + \tilde{\beta}\rho_g^2, \tag{33}$$

because both models have 6 parameters: H_0, Ω_k, Ω_b and 3 parameters in the EoS (27) or (33). It is convenient to use the critical density $\rho_{cr} = 3H_0^2/(8\pi G)$, introduce the dimensionless parameters $p_0 = \tilde{p}_0/\rho_{cr}$, $\beta = \tilde{\beta}\rho_{cr}$ instead of $\tilde{p}_0$, $\tilde{\beta}$ and rewrite Eq. (33) in the form

$$p_g = p_0\rho_{cr} + w_0\rho_g + \beta\rho_g^2/\rho_{cr}. \tag{34}$$

Similarly to the GCG and MCG models the model with quadratic EoS (33) or (34) has the analytical general solution of Eq. (19) [50]

$$\frac{\rho_g}{\rho_{cr}} = \begin{cases} \frac{1}{2\beta}\left[\frac{\Gamma-\sqrt{|\Delta|}\tan\left(\frac{3}{2}\sqrt{|\Delta|}\,\mathcal{A}\right)}{1+|\Delta|^{-1/2}\tan\left(\frac{3}{2}\sqrt{|\Delta|}\,\mathcal{A}\right)} - 1 - w_0\right], & \Delta < 0, \\ \frac{1}{2\beta}\left[\left(\frac{3}{2}\mathcal{A} + 1/\Gamma\right)^{-1} - 1 - w_0\right], & \Delta = 0, \\ \frac{\rho_-(\Omega_m-\rho_+)(a/a_0)^{-3\sqrt{\Delta}} - \rho_+(\Omega_m-\rho_-)}{(\Omega_m-\rho_+)(a/a_0)^{-3\sqrt{\Delta}} - \Omega_m + \rho_-}, & \Delta > 0, \end{cases} \tag{35}$$

depending on a sign of the discriminant $\Delta = (1+w_0)^2 - 4\beta p_0$. Here

$$\Omega_m = 1 - \Omega_k - \Omega_b, \quad \Gamma = 2\beta\Omega_m + 1 + w_0, \quad \rho_\pm = \frac{-1 - w_0 \pm \sqrt{\Delta}}{2\beta}, \quad \mathcal{A} = \log\frac{a}{a_0}.$$

The equation (18) for this model is reduced to the form

$$\frac{H^2}{H_0^2} = \left(\frac{d\mathcal{A}}{d\tau}\right)^2 = \frac{\rho_g}{\rho_{cr}} + \Omega_b e^{-3\mathcal{A}} + \Omega_k e^{-2\mathcal{A}}. \tag{36}$$

We solve this equation numerically from the present time initial condition $\mathcal{A}|_{\tau=1} = 0$ "to the past". We can use analytical solution (35) or solve Eq. (19) numerically, these approaches are equivalent.

For the model (34) the effective value

$$\Omega_m^{eff} = \Omega_b + p_0 + \Omega_m(1 + w_0 + \beta\Omega_m) \tag{37}$$

is calculated in the $z \to 0$ or $\mathcal{A} \to 0$ limit similarly to the MCG model.

The model with quadratic EoS (34) in the domain $\beta > 0$ may have the following singularity in the past: when $t \to t_* + 0$, density grows to infinity, but the scale factor remains finite and nonzero: $\lim\limits_{t\to t_*}\rho_g = \infty$, $\lim\limits_{t\to t_*} a = a(t_*) \neq 0$. This behavior resembles the Type III finite-time future singularity from the classification [36, 37]. In Ref. [53] the author did not see these singularities, because he considered only negative values $\beta = -(w_0+1)/\rho_P$.

In the bottom-right panel of figure 4 we present the example of singular solution as the red dashed line for $a(\tau)/a_0$ and the black dash-dotted line for $0.01 \cdot \rho(\tau)/\rho_{cr}$. This singularity is compared with the regular solution (the blue solid line for $a(\tau)/a_0$) with the optimal values of model parameters from table V. For the singular solution in this panel $\beta = 0.02$, but other model parameters are from table V.

We have to exclude these nonphysical singular solutions, for this purpose we can use different approaches. The simplest way is to add the penalty contribution in χ^2_Σ in the form

$$\Delta\chi^2_\Sigma = P_1[\exp(P_2 a(t_*)/a_0) - 1]. \tag{38}$$

The function (38) with $P_1 = 0.3$ and $P_2 = 20$ successfully helps to avoid this singularity. For regular solutions $a(t_*) = 0$ and the contribution (38) vanishes. In the top panels of figure 4 functions $\min\chi^2_\Sigma$ with the contribution (38) are shown as solid red lines for the formula (10) and as blue dashed lines for $r_d = (r_d h)_{fid} \cdot h^{-1}$; for the case without penalty (38) these graphs are dotted lines of the correspondent color: red for the formula (10) and blue for (11).

More natural method to eliminate nonphysical singular solutions is to include early time parameters (for example, z_d) into consideration. Unfortunately, both equations (10) and (11) or $r_s(z_d)$ are insensitive to the mentioned singularities. So we can take into account the cosmic microwave background (CMB) constraints, in particular, for the values [7]

$$\mathbf{v} = (\omega_b,\ \omega_{cb},\ D_M(1090)/r_d), \tag{39}$$

where $\omega_i = \omega_i h^2$, $D_M(z) = D_L(z)/(1+z)$. If we calculate the vector (39), compare it with the estimation [7, 8] $\Delta\mathbf{v} = \mathbf{v} - (0.02259,\ 0.1354,\ 94.51)$ and add the corresponding term to the χ^2_Σ function (24), we obtain

$$\chi^2_{\Sigma+} = \chi^2_\Sigma + \Delta\mathbf{v} \cdot C^{-1}_{CMB} (\Delta\mathbf{v})^T. \tag{40}$$

Here the covariance matrix from Ref. [7] contains $c_{11} = 2.864 \cdot 10^{-7}$, $c_{12} = -4.809 \cdot 10^{-7}$, $c_{13} = -1.111 \cdot 10^{-5}$, $c_{22} = 1.908 \cdot 10^{-5}$, $c_{23} = -7.495 \cdot 10^{-6}$, $c_{33} = 0.02542$.

Graphs of one parameter functions $\min\chi^2_{\Sigma+}$ with the CMB contribution for the case (10) are also presented in the top panels of figure 4 as black dash-dotted lines.

We demonstrate in figure 4 how the model (34) is effective in describing the observational data from Ref. [3] and tables II, III. Notations are the same as in figure 3. Here we also fix the value (12) $\Omega_b = 0.044$ (except for 2 top-right panels) and do not use Ω_b as a fitting parameter. The dependence $\min\chi^2_\Sigma(\Omega_b) = \min\limits_{H_0,\Omega_k,w_0,p_0,\beta} \chi^2_\Sigma$ (shown in the top-right panel) is rather weak for the case (11) $r_d = (r_d h)_{fid} \cdot h^{-1}$, but it is essential for the formula (10) and for the function $\min\chi^2_{\Sigma+}$. In the case $\min\chi^2_\Sigma$ with Eq. (10) (the red curve) the dependence $\min\chi^2_\Sigma(\Omega_b)$ is very close to the correspondents functions for the ΛCDM, GCG, MCG models in figures 1, 3; its minimum is also at $\Omega_b \simeq 0.044 \pm 0.004$.

In the top line panels of figure 4 we draw graphs of χ^2_Σ minima depending on one model parameter (H_0, $\Omega_k \ldots$) for the model (34) with the penalty function (38) as solid red lines for the formula (10) and as blue dashed lines for the case (11). Correspondent lines without contribution (38) are shown as dots of the same color. In other words, if we calculate $\min\chi^2_\Sigma$ only for (physical) regular solutions, we obtain the solid or dashed lines; for dots we also include singular solutions without physical interpretation. These lines coincide in domains where best values of β are negative and corresponding solutions are regular. One can see in figure 4 that optimal values of model parameters correspond to regular solutions in both considered cases (10) (table V) and (11) (table VI).

Minima of χ^2_Σ and $\chi^2_{\Sigma+}$ here have the same sense as in figure 3 for the MCG model, in particular, in the top-left panel $\min\chi^2_\Sigma(H_0) = \min\limits_{\Omega_k,w_0,p_0,\beta} \chi^2_\Sigma$. Dependence of this minimum on H_0 for two formulas for $r_s(z_d)$ resembles other considered models (compare with figures 2, 3): the graph for the case (11) is more sharp, than for Eq. (10), it corresponds to larger optimal value of H_0 and smaller 1σ error in table VI than the values in table V. For other panels of the top line in figure 4 dependence of $\min\chi^2_\Sigma$ on parameters Ω_k, w_0 and p_0 results in the correspondent the 1σ estimates in tables V, VI.

The functions $\min\chi^2_{\Sigma+}$ with the CMB contribution (40) depending on one parameter are shown as black dash-dotted lines in the top line panels. We see that the absolute minimum of this function is $\min\chi^2_{\Sigma+} \simeq 576.16$, in a bit exceeds the corresponding value $\min\chi^2_\Sigma \simeq 575.15$ for the case (10)

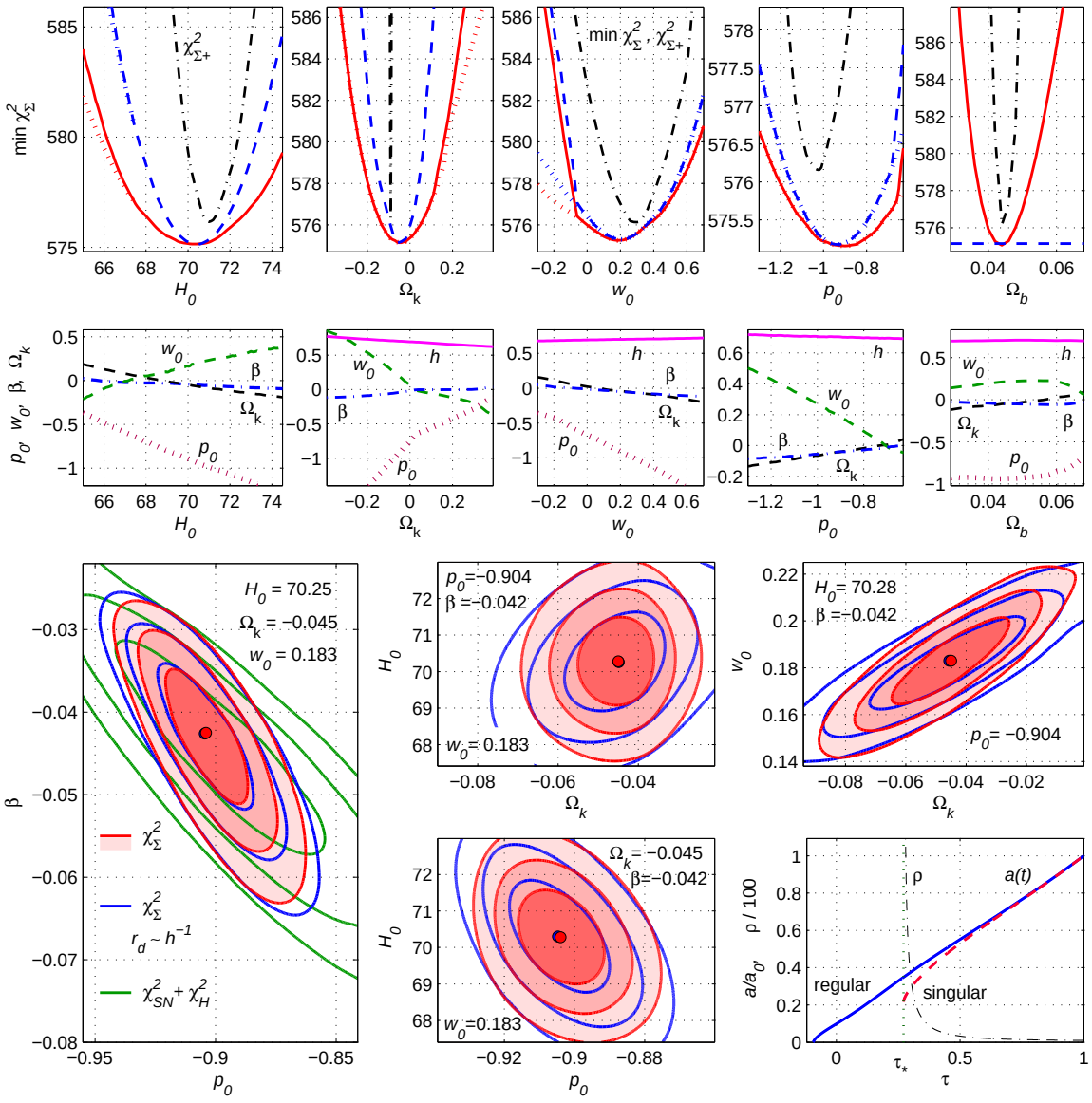

FIG. 4: For the model with quadratic EoS (34) one parameter dependencies of $\min\chi^2_\Sigma$ with $r_s(z_d)$ in the forms (10) (red solid lines) and (11) (blue dashed lines), of $\min\chi^2_\Sigma$ with CMB contribution and Eq. (10) (black dash-dotted lines) and also coordinates of minima points, level lines are presented in notations of figure 3. In the bottom-right panel scale factors $a/a(0)$ for the regular solution (the blue solid line) and the singular solution (the red dashed line) are shown.

in table V. However, the CMB contribution in the form (40) works as a very narrow filter for some model parameters, in particular, for the considered model with EoS (34) this contribution rigidly constrains the value Ω_k, so we have the $\chi^2_{\Sigma+}$ estimation $\Omega_k = -0.090 \pm 0.001$. The curve, corresponding to this narrow range, is shown in the second top panel of figure 4, it is too narrow, so it looks like a vertical black segment.

The $\chi^2_{\Sigma+}$ estimations of other parameters are also more narrow (see the top line in figure 4), than for both cases of χ^2_Σ, it is connected with restrictions for Ω_k and other correspondent parameters for other models. Some of these restrictions look like artificial od connected with the concrete choice of the CMB vector (39). So further we consider the functions $\min\chi^2_\Sigma$ without the CMB

contribution (40) with the fitting formula (10) as the most reliable indicator.

Panels in the second row of figure 4 correspond the upper panels for the function $\min \chi^2_\Sigma$ with the fitting formula (10) with the penalty contribution (38). They demonstrate evolution of coordinates of the minimal point if we vary the chosen parameter. In 4 bottom panels functions χ^2 depend on two model parameters $(p_0, \beta;\ p_0, H_0;\ \Omega_k, H_0;\ \Omega_k, w_0)$ when other parameters are fixed with their optimal values from table V. Red filled contours denote the case (10), blue lines corresponds to (11). These level lines demonstrate similarity with the MCG model in figure 3, but for the model (34) we have alternative behavior in the (Ω_k, H_0) plane. One should emphasize that all 1σ, 2σ and 3σ level lines for χ^2_Σ in figure 4 and optimal values of the model parameters in table V, VI lie in the domain with regular solutions of the quadratic EoS model (34).

VI. CONCLUSION

In this paper the Type Ia supernovae observational data from Ref. [3] and estimations of BAO parameters and $H(z)$ from tables II, III are described with the models ΛCDM, GCG (28), MCG (27) and the model with quadratic EoS (34). Two approaches in estimation of the sound horizon scale $r_s(z_d)$ are used and compared: the fitting formula (10) with results, tabulated in table V, and the expression (11) $r_d = (r_d h)_{fid} \cdot h^{-1}$ (table VI. Optimal values of model parameters with 1σ errors in these tables are calculated via one-parameter distributions (figures 2 – 4).

We also considered the CMB contribution in the form [7] (40), the results for the model with EoS (34) are shown in figure 4. However, this contribution appeared to be too sensitive and restrictive for some model parameters, in particular, Ω_k (or Ω_Λ for the ΛCDM model). So we consider the χ^2_Σ estimations of model parameters in tables V and VI as more reliable.

It is interesting that predictions of the ΛCDM, GCG, MCG models and the model with quadratic EoS for Ω_b are very close ($\Omega_b = 0.044 \pm 0.004$), if we adopt the fitting formula (10) for $r_s(z_d)$. We use this fact and do not consider Ω_b as an usual model parameter and fix its value in the form (12). One should note, that predictions of different models for H_0 and Ω_k in tables V and VI are also rather close.

Absolute minima of χ^2_Σ with the formula (10) in table V differ from the correspondent minima of in table VI with Eq. (11), but the hierarchy of all considered models is the same in these tables. In particular, the absolute minimum of χ^2_Σ in table V vary from the worst value 577.39 for the ΛCDM to the best result 575.15 for the model with quadratic EoS (34). Note that the advantage of the MCG model in comparison with GCG is larger in the case (11) in table VI.

However, effectiveness of a model essentially depends on its number N_p of model parameters (degrees of freedom). This number is used in model selection statistics, in particular, in the following Akaike information criterion [57, 60]

$$AIC = \min \chi^2_\Sigma + 2N_p.$$

If we fix the value Ω_b in the form (12) for the models GCG, MCG and with EoS (34) and do not use this parameter as a degree of freedom, we will have the numbers N_p and AIC for χ^2_Σ from table V for the considered models tabulated here in table VII.

This information criterion works against models with large N_p and adds arguments in favor of the ΛCDM model.

Acknowledgments

The work is supported by the Ministry of education and science of Russia, grant No. 1686. The author is grateful to S. D. Odintsov and E. G. Vorontsova for useful discussions, and to two

Model	$\min \chi^2_\Sigma$	N_p	AIC
ΛCDM	577.39	3	583.39
GCG	576.13	4	584.13
MCG	575.60	5	585.60
EoS (34)	575.15	5	585.15

TABLE VII: Akaike information criterion for the models.

unknown referees for valuable advices.

[1] A. G. Riess et al., *Astron. J.* **116** (1998) 1009, arXiv:astro-ph/9805201.
[2] S. Perlmutter et al., *Astrophys. J.* **517** (1999) 565, arXiv:astro-ph/9812133.
[3] N. Suzuki et al., *Astrophys. J.* **746** (2012) 85, arXiv:1105.3470 [astro-ph.CO]; http://supernova.lbl.gov/Union/.
[4] D. H. Weinberg et al., *Phys. Rep.* **530**, (2013) 87, arXiv: 1201.2434 [astro-ph.CO].
[5] D. J. Eisenstein et al., *Astrophys. J.* **633** (2005) 560, arXiv:astro-ph/0501171.
[6] D. J. Eisenstein and W. Hu, *Astrophys. J.* **496** (1998) 605, arXiv:astro-ph/9709112.
[7] E. Aubourg et al., *Phys. Rev. D* **92** (2015) 123516, arXiv:1411.1074 [astro-ph.CO].
[8] WMAP collaboration, G. Hinshaw et al., *Astrophys. J. Suppl.* **208** (2013) 19, arXiv:1212.5226 [astro-ph.CO].
[9] Planck Collaboration, P. A. R. Ade et al. *Astron. Astrophys.* **571** (2014) A16, arXiv:1303.5076 [astro-ph.CO].
[10] Planck Collaboration, P. A. R. Ade et al. arXiv:1502.01589 [astro-ph.CO].
[11] J. Simon, L. Verde and R. Jimenez, *Phys. Rev. D* **71** (2005) 123001, arXiv:astro-ph/0412269.
[12] D. Stern, R. Jimenez, L. Verde, M. Kamionkowski and S. A. Stanford, *J. Cosmol. Astropart. Phys.* **02** (2010) 008, arXiv:0907.3149 [astro-ph.CO].
[13] M. Moresco et al., *J. Cosmol. Astropart. Phys.* **8** (2012) 006, arXiv:1201.3609 [astro-ph.CO].
[14] C. Zhang et al., *Res. Astron. Astrophys.* **14** (2014) 1221, arXiv:1207.4541 [astro-ph.CO].
[15] M. Moresco, arXiv:1503.01116 [astro-ph.CO].
[16] E. Gaztañaga, A. Cabre, L. Hui, *Mon. Not. Roy. Astron. Soc.* **399(3)** (2009) 1663. arXiv:0807.3551 [astro-ph].
[17] C. Blake et al., *Mon. Not. Roy. Astron. Soc.* **425(1)** (2012) 405, arXiv:1204.3674 [astro-ph.CO].
[18] N. G. Busca et al., *Astron. and Astrop.* **552** (2013) A96 arXiv:1211.2616 [astro-ph.CO].
[19] C-H. Chuang and Y. Wang, *Mon. Not. Roy. Astron. Soc.* **435(1)** (2013) 255, arXiv:1209.0210 [astro-ph.CO].
[20] C-H. Chuang et al., *Mon. Not. Roy. Astron. Soc.* **433(4)** (2013) 3559, arXiv:1303.4486 [astro-ph.CO].
[21] L. Anderson et al., *Mon. Not. Roy. Astron. Soc.* **439(1)** (2014) 83, arXiv:1303.4666 [astro-ph.CO].
[22] L. Anderson et al., *Mon. Not. Roy. Astron. Soc.* **441** (2014) 24, arXiv:1312.4877 [astro-ph.CO].
[23] A. Oka et al., *Mon. Not. Roy. Astron. Soc.* **439(3)** (2014) 2515, arXiv:1310.2820 [astro-ph.CO].
[24] A. Font-Ribera et al., *J. Cosmol. Astropart. Phys.* **05** (2014) 027, arXiv:1311.1767 [astro-ph.CO].
[25] T. Delubac et al., *Astron. and Astrop.* **574** (2015) A59, arXiv:1404.1801 [astro-ph.CO].
[26] W. J. Percival et al.,*Mon. Not. Roy. Astron. Soc.* **401** (2010) 2148, arXiv:0907.1660 [astro-ph.CO].
[27] E. A. Kazin et al., *Astrophys. J.* **710** (2010) 1444, arXiv:0908.2598 [astro-ph.CO].
[28] F. Beutler et al., *Mon. Not. Roy. Astron. Soc.* **416** (2011) 3017, arXiv:1106.3366 [astro-ph.CO].
[29] C. Blake et al., *Mon. Not. Roy. Astron. Soc.* **418** (2011) 1707, arXiv:1108.2635 [astro-ph.CO].
[30] N. Padmanabhan et al., *Mon. Not. Roy. Astron. Soc.* **427** (2012) 2132, arXiv:1202.0090 [astro-ph.CO].
[31] H.-J. Seo et al., *Astrophys. J.* **761** (2012) 13, arXiv:1201.2172 [astro-ph.CO].
[32] E. A. Kazin et al., *Mon. Not. Roy. Astron. Soc.* **441** (2014) 3524, arXiv:1401.0358 [astro-ph.CO].
[33] A. J. Ross et al., *Mon. Not. Roy. Astron. Soc.* **449** (2015) 835, arXiv:1409.3242 [astro-ph.CO].
[34] E. J. Copeland, M. Sami and S. Tsujikawa, *Int. J. Mod. Phys. D* **15** (2006) 1753, hep-th/0603057.
[35] T. Clifton, P. G. Ferreira, A. Padilla and C. Skordis, *Physics Reports* **513** (2012) 1, arXiv:1106.2476

[astro-ph.CO].
[36] K. Bamba, S. Capozziello, S. Nojiri and S. D. Odintsov, *Astrophys. and Space Science* **342** (2012) 155, arXiv:1205.3421 [gr-qc].
[37] S. Nojiri and S. D. Odintsov, *Phys. Rept.* **505** (2011) 59, arXiv:1011.0544 [gr-qc].
[38] O. A. Grigorieva and G. S. Sharov, *Int. J. Mod. Phys. D* **22** (2013) 1350075, arXiv:1211.4992, [gr-qc].
[39] G. S. Sharov and E. G. Vorontsova, *J. Cosmol. Astropart. Phys.* **10** (2014) 057, arXiv:1407.5405, [gr-qc].
[40] A. Y. Kamenshchik, U. Moschella and V. Pasquier, *Phys. Lett. B* **511(2-4)** (2001) 265, arXiv:gr-qc/0103004.
[41] H. B. Benaoum, arXiv:hep-th/0205140.
[42] L. P. Chimento, *Phys. Rev. D.* **69** (2004) 123517.
[43] U. Debnath, A. Banerjee, S. Chakraborty, *Class. Quant. Grav.* **21** (2004) 5609, arXiv:gr-qc/0411015.
[44] D-J. Liu, X-Z. Li, *Chin. Phys. Lett.* **22** (2005) 1600, astro-ph/0501115.
[45] J. Lu, L. Xu, Y. Wu and M. Liu, *Gen. Rel. Grav.* **43** (2011) 819, arXiv:1105.1870 [astro-ph.CO].
[46] B. C. Paul and P. Thakur, *J. Cosmol. Astropart. Phys.* **11** (2013) 052, arXiv:1306.4808 [astro-ph.CO].
[47] B.C. Paul, P. Thakur and A. Beesham, arXiv:1410.6588 [astro-ph.CO].
[48] S. Nojiri and S. D. Odintsov, *Phys. Rev. D* **70** (2004) 103522, arXiv:hep-th/0408170.
[49] S. Nojiri, S. D. Odintsov and S. Tsujikawa, *Phys. Rev. D* **71** (2005) 063004, arXiv:hep-th/0501025.
[50] K. N. Ananda and M. Bruni, *Phys. Rev. D* **74** (2006) 023523, arXiv:astro-ph/0512224.
[51] E. V. Linder and R. J. Scherrer, *Phys. Rev. D* **80** (2009) 023008, arXiv:0811.2797 [astro-ph].
[52] A. V. Astashenok, S. Nojiri, S. D. Odintsov and A. V. Yurov, *Phys. Lett. B* **709** (2012) 396, arXiv:1201.4056 [gr-qc].
[53] P-H. Chavanis, arXiv:1309.5784 [astro-ph.CO].
[54] S. Nesseris and L. Perivolaropoulos, *Phys. Rev. D* **72** (2005) 123519, arXiv:astro-ph/0511040.
[55] O. Farooq, D. Mania and B. Ratra, *Astrophys. J.* **764** (2013) 139, arXiv:1211.4253 [astro-ph.CO].
[56] O. Farooq and B. Ratra, *Astrophys. J.* **766** (2013) L7, arXiv:1301.5243 [astro-ph.CO].
[57] K. Shi, Y. F. Huang and T. Lu, *Monthly Notices Roy. Astron. Soc.* **426** (2012) 2452, arXiv:1207.5875 [astro-ph.CO].
[58] A. G. Riess et al., *Astrophys. J.* **730(2)** (2011) 119, arXiv:1103.2976 [astro-ph.CO].
[59] M. C. Bento, O. Bertolami and A. A. Sen, *Phys. Rev. D* **66(4)** (2002) 043507, arXiv:gr-qc/0202064.
[60] M. Szydłowski, A. Kurek and A. Krawiec, *Phys. Lett. B* **642** (2006) 171, arXiv:astro-ph/0604327.